Science Advances
AAAS

Supplementary Materials for

Notch3 directs differentiation of brain mural cells from human pluripotent stem cell–derived neural crest

Benjamin D. Gastfriend *et al.*

Corresponding author: Eric V. Shusta, eshusta@wisc.edu; Sean P. Palecek, sppalecek@wisc.edu

Sci. Adv. **10**, eadi1737 (2024)
DOI: 10.1126/sciadv.adi1737

The PDF file includes:

Other Supplementary Material for this manuscript includes the following:

Table S1. Published datasets used.

Reference	Description	Source	Accession Numbers/Identifiers
(*43*)	hPSC-derived brain pericyte-like cells	https://www.ncbi.nlm.nih.gov/geo/query/acc.cgi?acc=GSE124579	GSM3537065 (SRR8385490, SRR8385491) GSM3537067 (SRR8385494, SRR8385495) GSM3537068 (SRR8385496, SRR8385497) GSM3537069 (SRR8385498, SRR8385499) GSM3537070 (SRR8385500, SRR8385501)
(*45*)	hPSC-derived brain pericyte-like cells	https://www.ncbi.nlm.nih.gov/geo/query/acc.cgi?acc=GSE104141	GSM2790557 (SRR6059668) GSM2790558 (SRR6059669) GSM2790559 (SRR6059670)
(*46*)	hPSC-derived brain pericyte-like cells	https://www.ncbi.nlm.nih.gov/geo/query/acc.cgi?acc=GSE132857	GSM3895132 (SRR9312712) GSM3895133 (SRR9312713) GSM3895134 (SRR9312714) GSM3895135 (SRR9312715)
(*48*)	Mouse developing brain scRNA-seq	http://mousebrain.org/development/downloads.html	dev_all.loom
(*41*)	Meta-analysis of human brain scRNA-seq datasets (enumerated below)		
(*88*)	Adult human neocortex scRNA-seq	https://portal.brain-map.org/atlases-and-data/rnaseq/human-multiple-cortical-areas-smart-seq	
(*89*)	GW17-18 human neocortex scRNA-seq	http://solo.bmap.ucla.edu/shiny/webapp/	
(*91*)	Adult human temporal lobe and cerebellum scRNA-seq	https://www.ncbi.nlm.nih.gov/geo/query/acc.cgi?acc=GSE134355	GSM3980129, GSM4008656, GSM4008657, GSM4008658
(*90*)	GW6-11 human ventral midbrain scRNA-seq	https://www.ncbi.nlm.nih.gov/geo/query/acc.cgi?acc=GSE76381	
(*92*)	GW16-27 human hippocampus scRNA-seq	https://www.ncbi.nlm.nih.gov/geo/query/acc.cgi?acc=GSE119212	

Table S2. Antibodies.

Target	Species/ isotype	Manufacturer, clone (product number), RRID	Fluorophore	App.[a]	Dilution
p75-NGFR	Mouse IgG1	Advanced Targeting Systems, ME20.4 (AB-N07) RRID:AB_171797	Unconjugated	FC	0.2 µL / 10^6 cells
HNK-1	Mouse IgM	Sigma-Aldrich, VC1.1 (C6680) RRID:AB_1078474	Unconjugated	FC	0.2 µL / 10^6 cells
PDGFRβ	Rabbit IgG	Cell Signaling Technology, 28E1 (3169) RRID:AB_2162497	Unconjugated	ICC	1:100
				WB	1:500
Notch3	Rabbit IgG	Cell Signaling Technology, D11B8 (5276) RRID:AB_10560515	Unconjugated	ICC	1:100
				WB	1:1000
				IP	1:200
				ChIP	1:200
Isotype control	Rabbit IgG	Cell Signaling Technology, DA1E (3900) RRID:AB_1550038	Unconjugated	IP	1:688
Notch1	Rabbit IgG	Cell Signaling Technology, D1E11 (3608) RRID:AB_2153354	Unconjugated	WB	1:1000
VE-cadherin	Mouse IgG2a	Santa Cruz, BV9 (sc-52751) RRID:AB_628919	Unconjugated	ICC	1:100
Tbx2	Rabbit polyclonal	Prestige Antibodies, (HPA008586) RRID:AB_1080222	Unconjugated	ICC	1:100
				WB	1:500
Fibronectin	Mouse IgG1	Santa Cruz, EP5 (sc-8422) RRID:AB_627598	Unconjugated	ICC	1:50
				WB	1:250
GFP	Mouse IgG2a	Santa Cruz, B-2 (sc-9996) RRID:AB_627695	Unconjugated	ICC	1:50
				WB	1:250
Calponin	Mouse IgG1	Sigma-Aldrich, hCP (C2687) RRID:AB_476840	Unconjugated	ICC	1:15,000
SM22α	Rabbit polyclonal	Abcam, (ab14106) RRID:AB_443021	Unconjugated	ICC	1:1000
α-SMA	Mouse IgG2a	Lab Vision, 1A4 (MS-113-P) RRID:AB_64000	Unconjugated	ICC	1:100
RBPJ	Rabbit IgG	Cell Signaling Technology, D10A4 (5313) RRID:AB_2665555	Unconjugated	WB	1:1000
β-actin	Rabbit IgG	Cell Signaling Technology, 13E5 (4970) RRID:AB_2223172	Unconjugated	WB	1:1000
Rabbit IgG (conformation-specific)	Mouse IgG	Cell Signaling Technology, L27A9 (3678) RRID: RRID:AB_1549606	Unconjugated	WB	1:2000

Rabbit IgG	Goat polyclonal	LI-COR, (925-68071) RRID:AB_10956166	IRDye 680RD	WB	1:5000
Mouse IgG	Goat polyclonal	LI-COR, (926-68070) RRID:AB_10956588	IRDye 680RD	WB	1:5000
Rabbit IgG	Goat polyclonal	LI-COR, (926-32211) RRID:AB_621843	IRDye 800CW	WB	1:5000
Mouse IgG	Goat polyclonal	LI-COR, (926-32210) RRID:AB_621842	IRDye 800CW	WB	1:5000
Mouse IgG1	Goat polyclonal	Invitrogen, (A-21240) RRID:AB_2535809	Alexa Fluor 647	FC	1:500
Mouse IgM	Goat polyclonal	Invitrogen, (A-21042) RRID:AB_2535711	Alexa Fluor 488	FC	1:500
Rabbit IgG	Goat polyclonal	Invitrogen, (A-21245) RRID:AB_2535813	Alexa Fluor 647	ICC	1:200
Mouse IgG	Goat polyclonal	Invitrogen, (A-21235) RRID:AB_2535804	Alexa Fluor 647	ICC	1:200
Mouse IgG	Goat polyclonal	Invitrogen, (A-11001) RRID:AB_2534069	Alexa Fluor 488	ICC	1:200
Mouse IgG	Goat polyclonal	Invitrogen, (A-21424) RRID:AB_141780	Alexa Fluor 555	ICC	1:200

[a]Application: FC, Flow cytometry; ICC, immunocytochemistry; WB, Western blotting; IP, immunoprecipitation; ChIP: chromatin immunoprecipitation

Table S3. Primer sequences.

Gene	Primer sequence
Primers for cloning	
NOTCH3 forward	TAA GCA TTA ATT AAG CCA CCA TGG TCA TGG TGG CCC GG
NOTCH3 reverse	TGC TTA TTA ATT AAT CAG GCC AAC ACT TGC C
NOTCH1 forward	TAA GCA TTA ATT AAG CCA CCA TGG TGC TGC TGT CCC GCA AGC G
NOTCH1 reverse	TGC TTA TTA ATT AAT TAC TTG AAG GCC TCC GGA A
TBX2 forward	TAA GCA TTA ATT AAG CCA CCA TGA GAG AGC CGG CGC
TBX2 reverse	TGC TTA TTA ATT AAT CAC TTG GGC GAC TCC C
EF-1α promoter forward	TCA AGC CTC AGA CAG TGG TTC
IRES reverse	CCT CAC ATT GCC AAA AGA CG
Primers for RT-qPCR	
eGFP forward	GAA CCG CAT CGA GCT GAA
eGFP reverse	TGC TTG TCG GCC ATG ATA TAG
ACTB forward	CAT CCG CAA AGA CCT GTA CG
ACTB reverse	CCT GCT TGC TGA TCC ACA TC
NGFR forward	GTG GGA CAG AGT CTG GGT GT
NGFR reverse	AAG GAG GGG AGG TGA TAG GA
PDGFRB forward	GCT CAC CAT CAT CTC CCT TAT C
PDGFRB reverse	CTC ACA GAC TCA ATC ACC TTC C
RGS5 forward	GGA GGC TCC TAA AGA GGT GAA TA
RGS5 reverse	CCA TCA GGG CAT GGA TTC TTT
KCNJ8 forward	AAC CTG GCG CAT AAG AAC ATC
KCNJ8 reverse	CCA CAT GAT AGC GAA GAG CAG
NOTCH3 forward[a]	GAG ACG CTC GTC AGT TCT TAG
NOTCH3 reverse[a]	GGT GGA AAG AGA AGA GGA TGA A
TBX2 forward	ACA TCC TGA AGC TGC CTT AC
TBX2 reverse	AGC TGT GTG ATC TTG TCA TTC T
HEYL forward	CAG ATG CAA GCC AGG AAG AA
HEYL reverse	GGA AGA GCC CTG TTT CTC AAA
FOXS1 forward	CCA AGG ACA ACC ACA CAG AA
FOXS1 reverse	GCC ACA GAG TAA ATC CCA AGA G
TBX18 forward	CCC AGG ACT CCC TCC TAT GT
TBX18 reverse	TAG GAA CCC TGA TGG GTC TG
FOXF2 forward[b]	ACC AGA GCG TCT GTC AGG ATA TT
FOXF2 reverse[b]	GTG ACT TGA ATC CGT CCC AGT TTC
MYL9 forward	GTC CCA GAT CCA GGA GTT TAA G
MYL9 reverse	CAT CAT GCC CTC CAG GTA TT
NDUFA4L2 forward	AGA GGA CCA GAC TGG GAA A
NDUFA4L2 reverse	CAG GCA GAT TAA GCC GAT CA
HIGD1B forward	CGA AGA CTG TGT GTC TGA GAA G
HIGD1B reverse	CTC AGC CGG TAA ATC CTG TAT G
ACTA2 forward	TGT TCC AGC CAT CCT TCA TC
ACTA2 reverse	GCA ATG CCA GGG TAC ATA GT

[a]Primers target 3'UTR and thus do not amplify transgene-derived transcripts.
[b]From ref. (*110*)

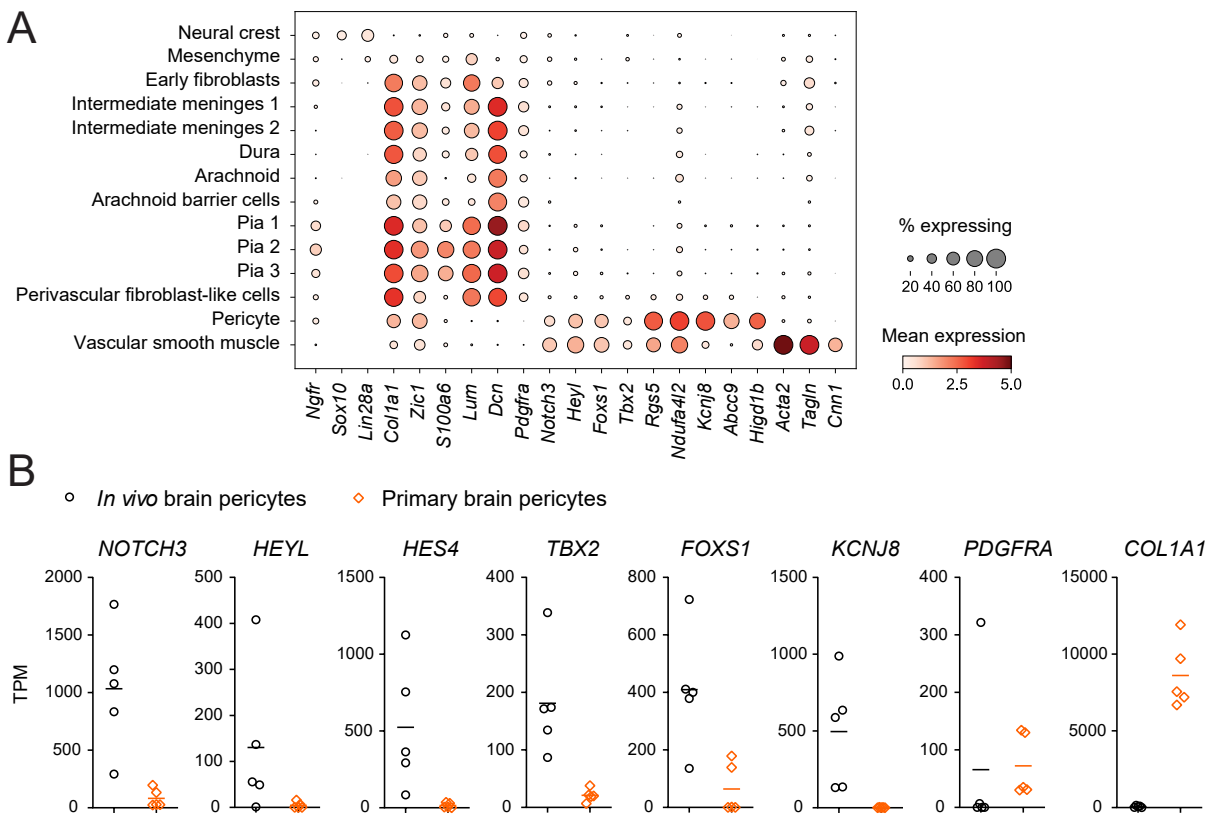

Figure S1. Markers of neural crest, mural cells, and other mesenchymal derivatives. (A) Dot plot of gene expression in murine cell Subclasses as defined by the authors. Neural crest, pan-mesenchymal, fibroblast, pan-mural, pericyte, and VSMC marker genes are shown. Color indicates expression level and dot size indicates the percent of cells in the indicated Subclass that express a given gene. Data from (*48*). **(B)** Transcript abundance of selected genes from *in vivo* human brain pericytes and primary human brain pericytes (*41*). Data for *in vivo* human brain pericytes are the same as shown in Fig. 1B. TPM: transcripts per million.

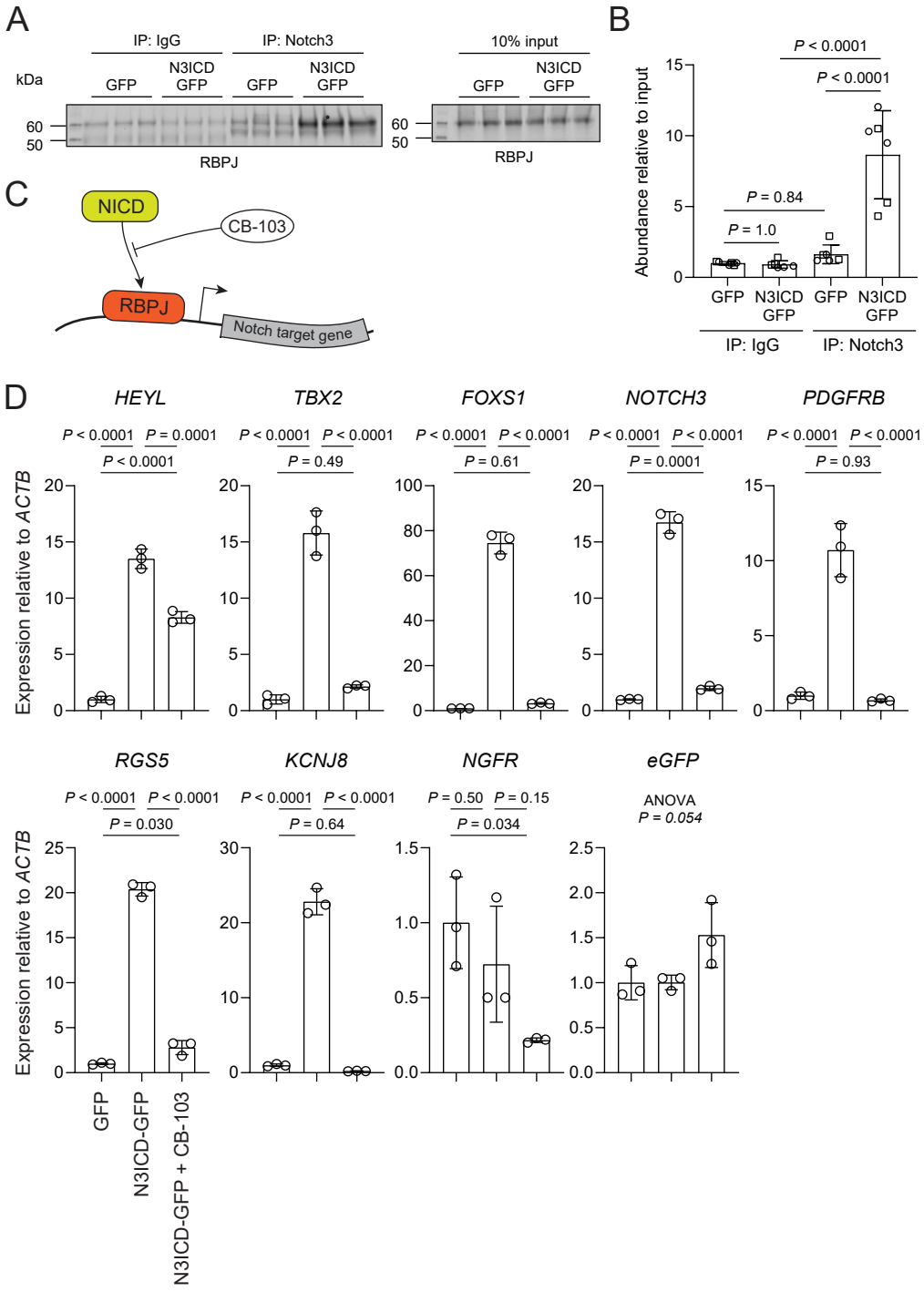

Figure S2. Notch-dependence of observed transcriptional changes. **(A)** Western blots of isotype control IgG and Notch3 immunoprecipitates (top) and input controls (bottom) from cells 6 days after transduction with GFP or N3ICD-GFP lentiviruses. Membranes were probed with the RBPJ antibody. **(B)** Quantification of Western blots from co-immunoprecipitation assay described

in (A). RBPJ band intensities from immunoprecipitates were normalized to respective input control band intensities. Points represent replicate wells from two differentiations of the H9 hPSC line, each differentiation indicated with a different shape. Bars indicate mean values ± SD, with values normalized within each differentiation such that the mean of the GFP, IP: IgG condition equals 1. P-values: Two-way ANOVA on unnormalized data followed by Tukey's HSD test. **(C)** Schematic of the mechanism of action of CB-103, a small molecule inhibitor of the Notch transcriptional activation complex (*49*). NICD: Notch intracellular domain. **(D)** RT-qPCR analysis of mural cell gene expression 6 days after transduction of neural crest cells with GFP or N3ICD-GFP lentiviruses. Expression of each gene is shown relative to *ACTB* expression and normalized to expression in GFP-transduced cells. Points represent replicate wells from a differentiation of the H9 hPSC line and bars indicate mean ± SD. P-values: ANOVA followed by Tukey's HSD test.

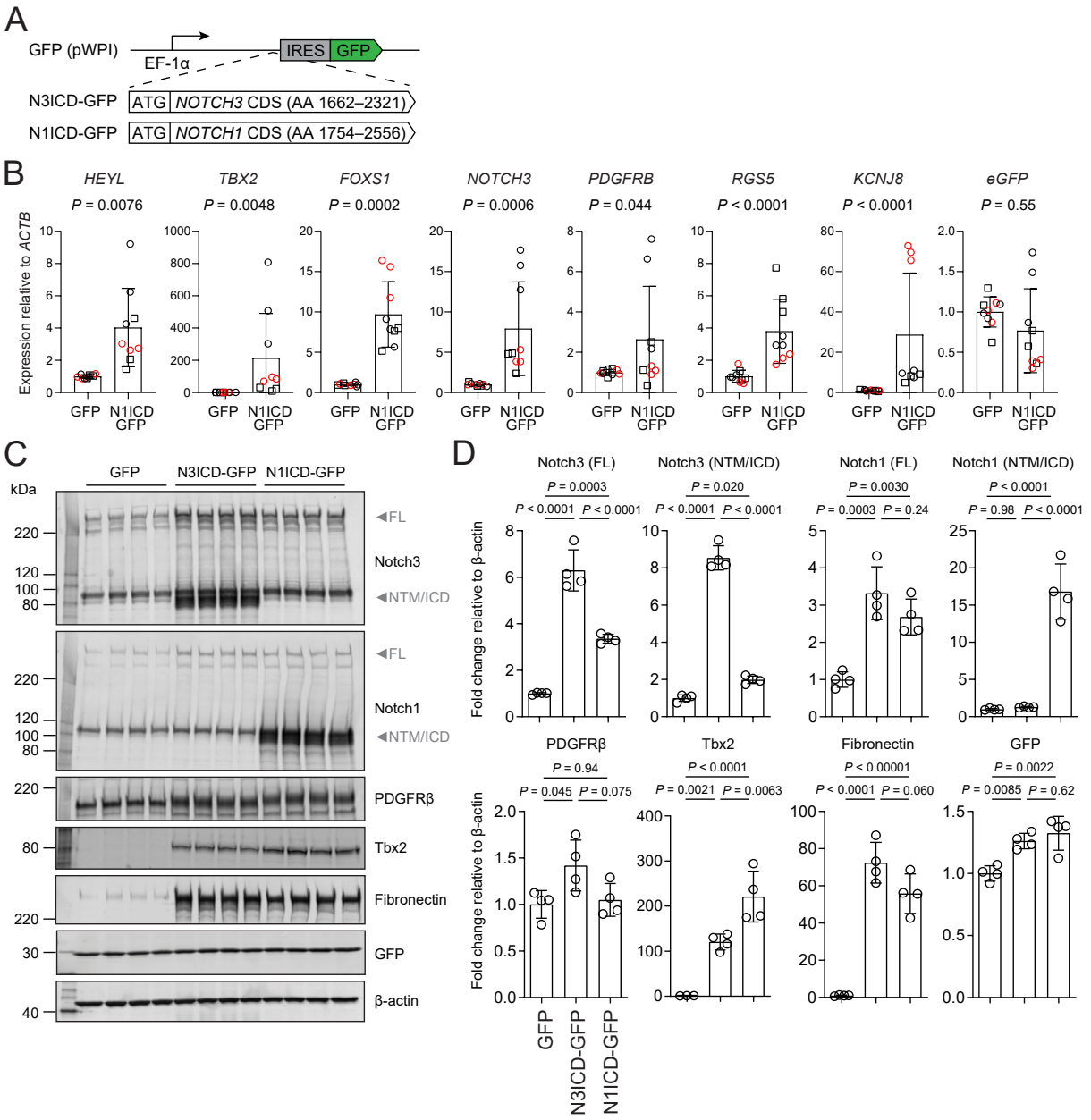

Figure S3. Effects of N1ICD and N3ICD overexpression. (A) Schematic of lentiviral overexpression constructs. The parental pWPI vector and N3ICD-GFP are as described in Figure 1. To generate N1ICD-GFP, a fragment of the human *NOTCH1* coding sequence (CDS) encoding the intracellular domain of Notch1 was cloned into pWPI. IRES: internal ribosome entry site; AA: amino acids. **(B)** RT-qPCR analysis of mural cell gene expression 6 days after transduction of neural crest cells with GFP or N1ICD-GFP lentiviruses. Expression of each gene is shown relative

to *ACTB* expression. Points represent replicate wells from three independent differentiations, two in the H9 hPSC line (black circles, black squares) and one in the IMR90-4 hPSC line (red circles). Bars indicate mean values ± SD, with values normalized within each differentiation such that the mean of the GFP condition equals 1. P-values: Two-way ANOVA on unnormalized data. **(C)** Western blots of cells 6 days after transduction with GFP, N3ICD-GFP, or N1ICD-GFP lentiviruses. Membranes were probed with Notch3, Notch1, PDGFRβ, Tbx2, fibronectin, GFP, and β-actin antibodies. On the Notch3 and Notch1 Western blots, arrows indicate the full-length (FL) and Notch transmembrane/intracellular domain (NTM/ICD) bands. **(D)** Quantification of Western blots. Band intensities were normalized to β-actin band intensities. Points represent replicate wells from a differentiation of the H9 hPSC line. Bars indicate mean values ± SD, with values normalized such that the mean of the DMSO condition equals 1. P-values: ANOVA followed by Tukey's HSD test.

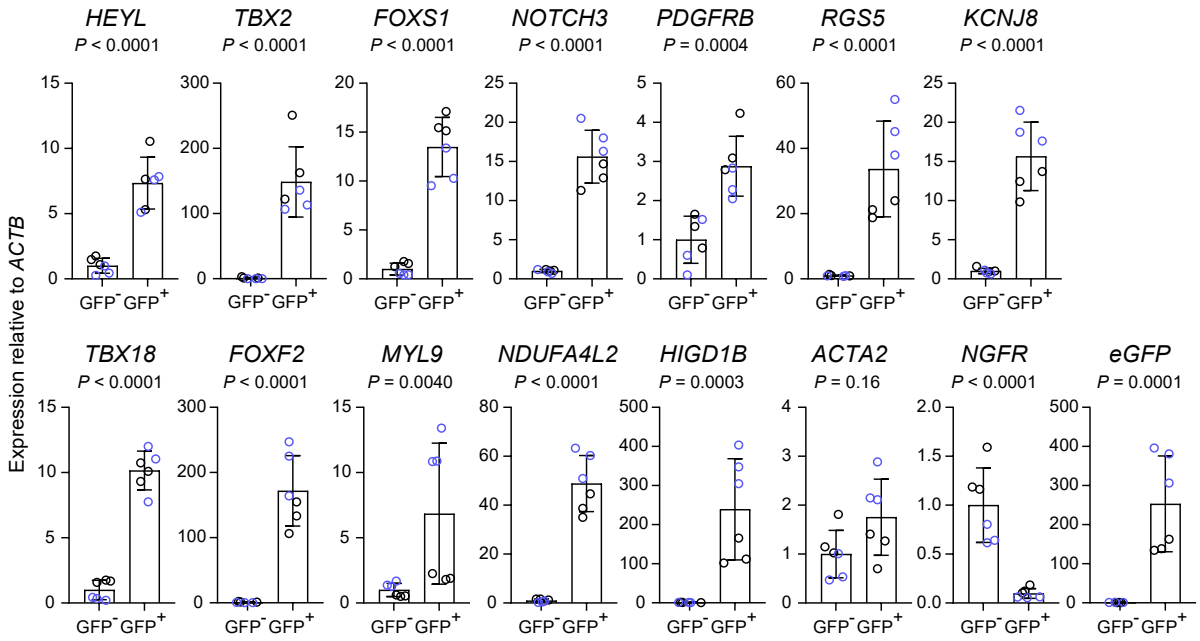

Figure S4. Cell-autonomous effects of N3ICD overexpression. RT-qPCR analysis of GFP$^-$ and GFP$^+$ cells isolated via FACS 6 days after transduction of neural crest cultures with N3ICD-GFP lentivirus. Expression of each gene is shown relative to *ACTB* expression and normalized to expression in GFP$^-$ cells. *NOTCH3* primers target the 3'UTR and thus amplify only endogenous *NOTCH3* transcripts. Points represent replicate wells from two independent differentiations, one in the H9 hPSC line (black circles) and one in the WTC11 hPSC line (blue circles). Bars indicate mean values ± SD. P-values: Two-way ANOVA.

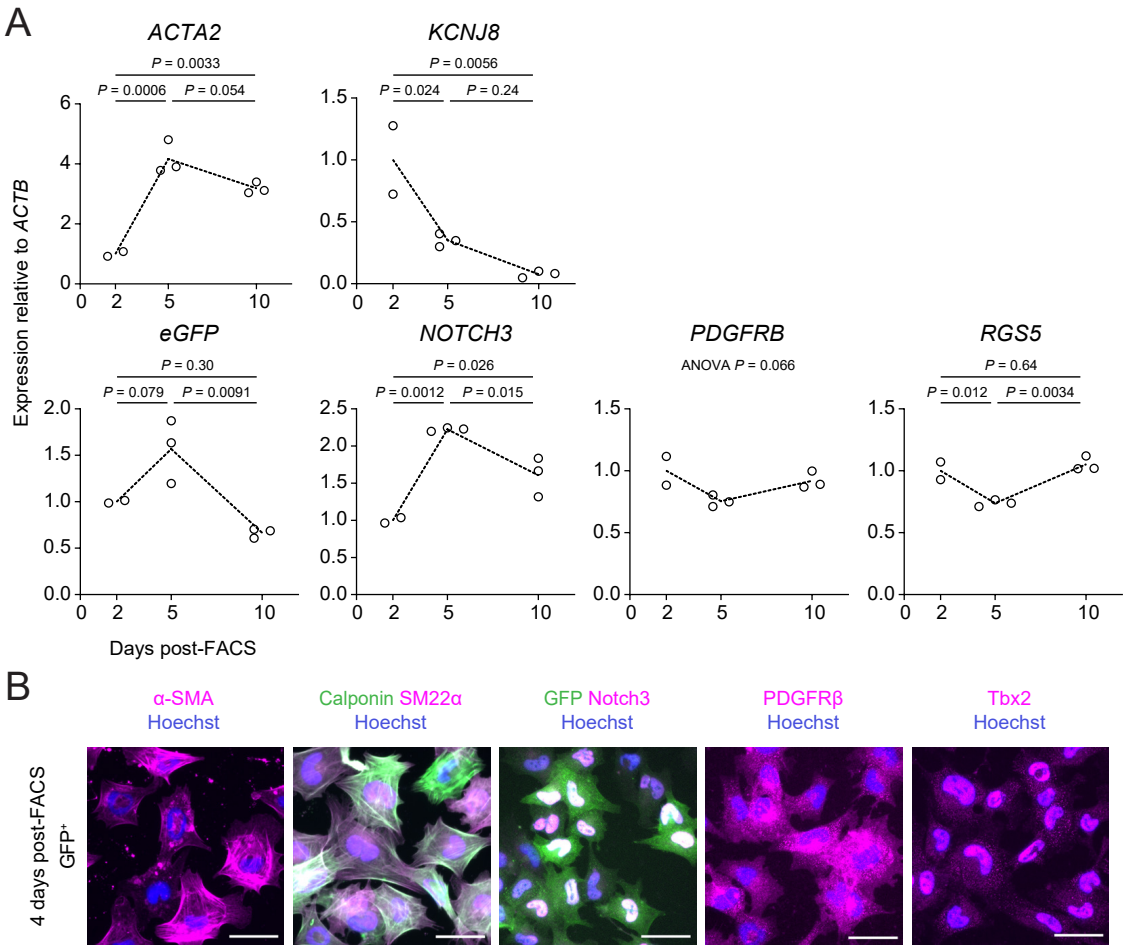

Figure S5. Differentiation of smooth muscle-like cells from N3ICD-derived mural cells by extended culture in E6 medium. (A) RT-qPCR analysis of GFP$^+$ cells at 2, 5, and 10 days after isolation via FACS and culture in E6 medium. FACS was performed 6 days after transduction of neural crest cultures with N3ICD-GFP lentivirus. Expression of each gene is shown relative to *ACTB* expression and normalized to expression at 2 days post-FACS. *NOTCH3* primers target the 3'UTR and thus amplify only endogenous *NOTCH3* transcripts. Points represent replicate wells from a differentiation of the H9 hPSC line. P-values: ANOVA followed by Tukey's HSD test. **(B)** Immunocytochemistry analysis of α-SMA, calponin, SM22α, PDGFRβ, Tbx2, Notch3, and GFP expression in GFP$^+$ cells from the H9 hPSC line 4 days after isolation via FACS as described above. Hoechst nuclear counterstain overlaid in all images. Scale bars: 50 μm.

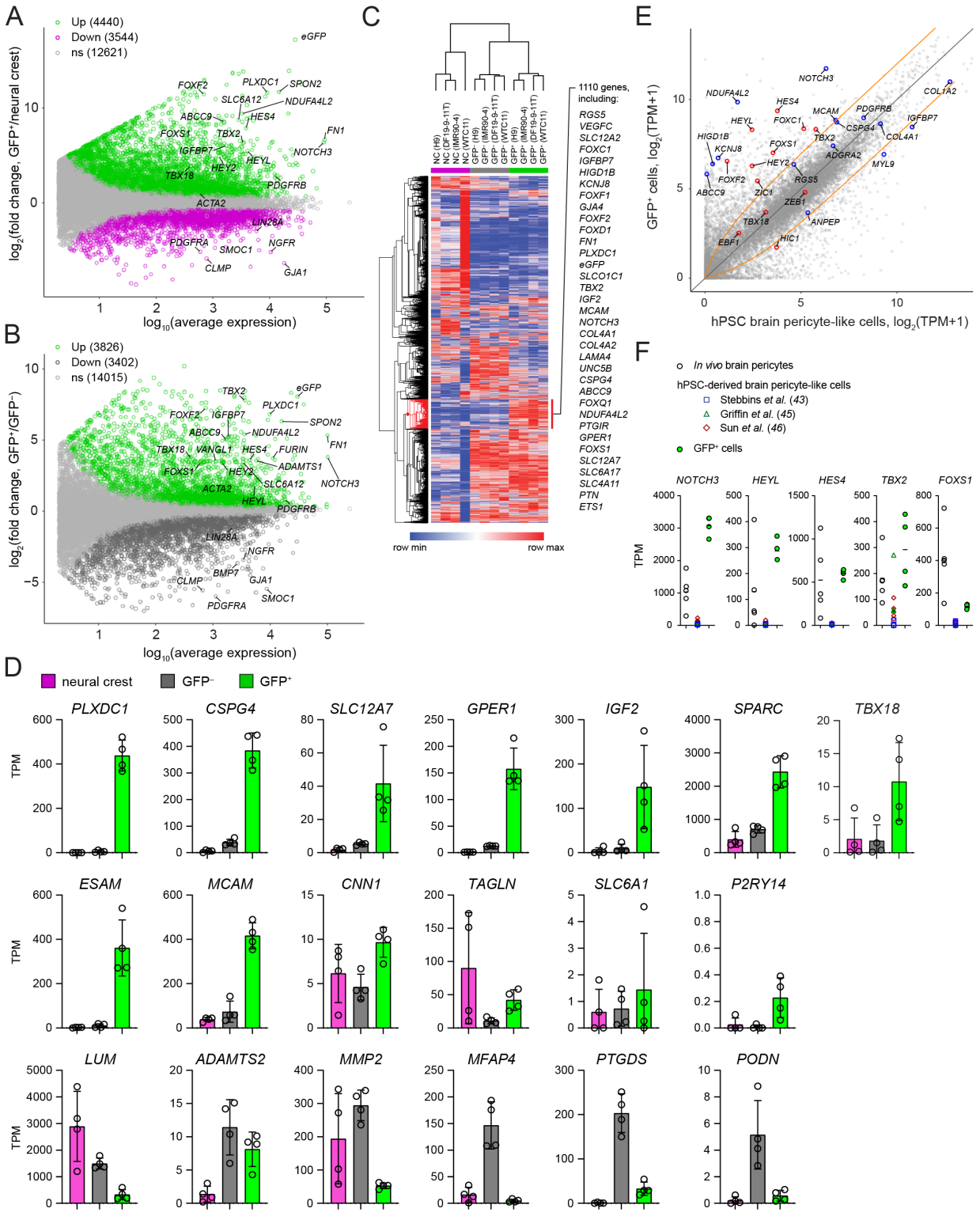

Figure S6. RNA-seq differential expression analysis and clustering. (A, B) Differential expression analysis of GFP$^+$ cells compared to neural crest (A) and GFP$^+$ cells compared to GFP$^-$

cells (B). Data are displayed in MA plots; volcano plots are shown in Fig. 3C-D. Differentially expressed genes (adjusted P-values < 0.05, DESeq2 Wald test with Benjamini-Hochberg correction) are highlighted, and the numbers of upregulated and downregulated genes are shown in the legends. Complete results of differential expression analysis are provided in File S2. **(C)** Hierarchical clustering of samples and genes. The red-colored portion of the dendrogram at left indicates a 1110-gene module exhibiting selective expression in GFP^+ cells compared to both $GFP^–$ cells and neural crest. Selected genes from this module are displayed at right and the complete list is provided in File S2. **(D)** Transcript abundance (TPM) of selected mural cell-enriched transcripts. Abundance data for all genes are provided in File S1. **(E)** Comparison of protein-coding transcript abundances in GFP^+ cells and hPSC-derived brain pericyte-like cells (the same data described in Fig. 1A) (*43*, *45*, *46*). Genes of interest are annotated in red (transcription factors) or blue (others). Orange lines represent fold changes of ±2. **(F)** Transcript abundance of selected genes from *in vivo* human brain pericytes (*41*), hPSC-derived brain pericyte-like cells (*43*, *45*, *46*), and GFP^+ cells. Bars indicate mean values. Data for *in vivo* human brain pericytes and hPSC-derived brain pericyte-like cells are the same as shown in Fig. 1B. TPM: transcripts per million.

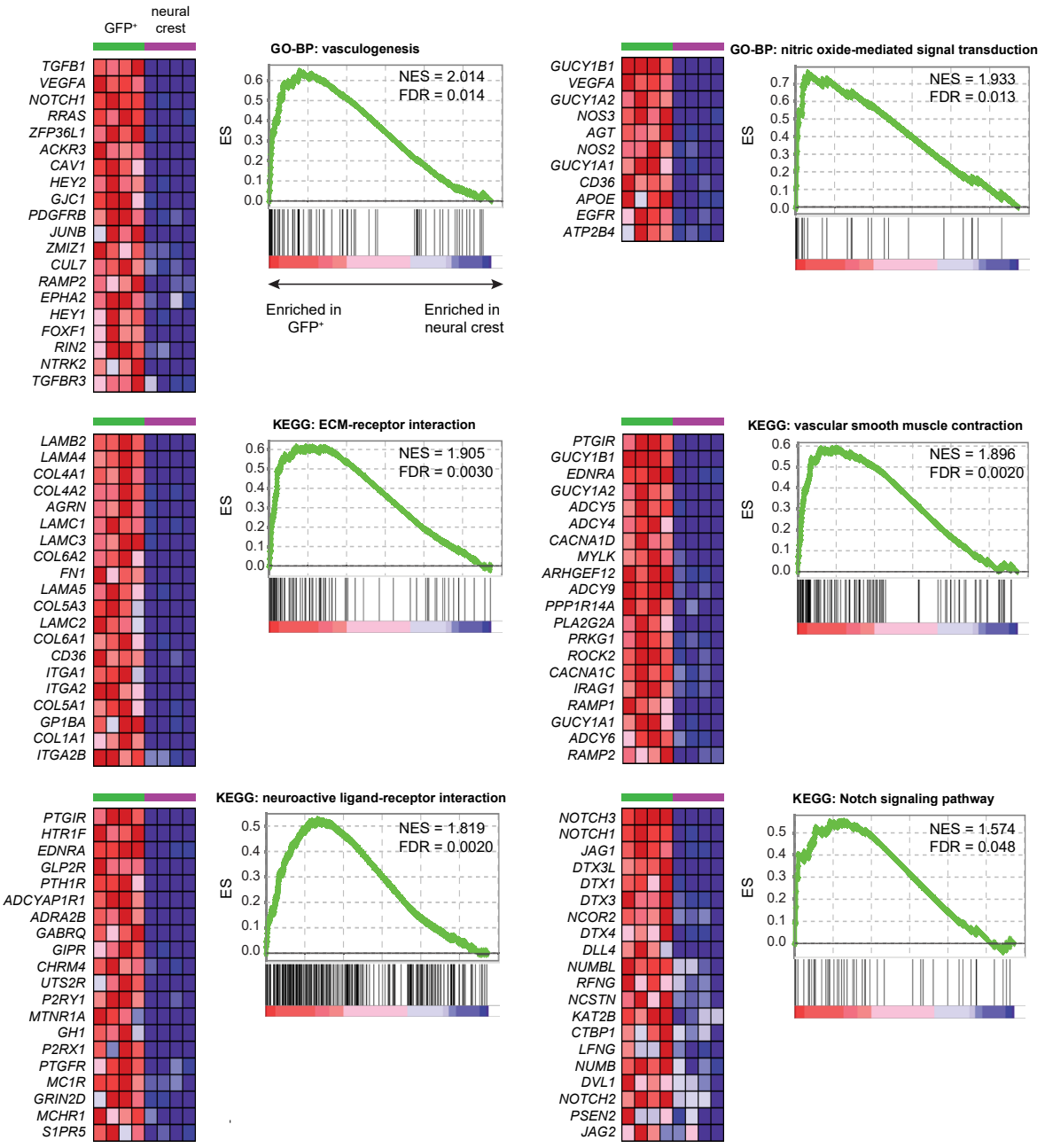

Figure S7. Gene set enrichment analysis. Gene sets enriched in GFP$^+$ cells compared to neural crest. GSEA enrichment plots for 6 gene sets of interest are shown. For each gene set, plots at left display normalized expression of up to 20 genes listed as core enrichments for each gene set, in order of GSEA rank. NES: normalized enrichment score. Complete GSEA results are provided in File S2.

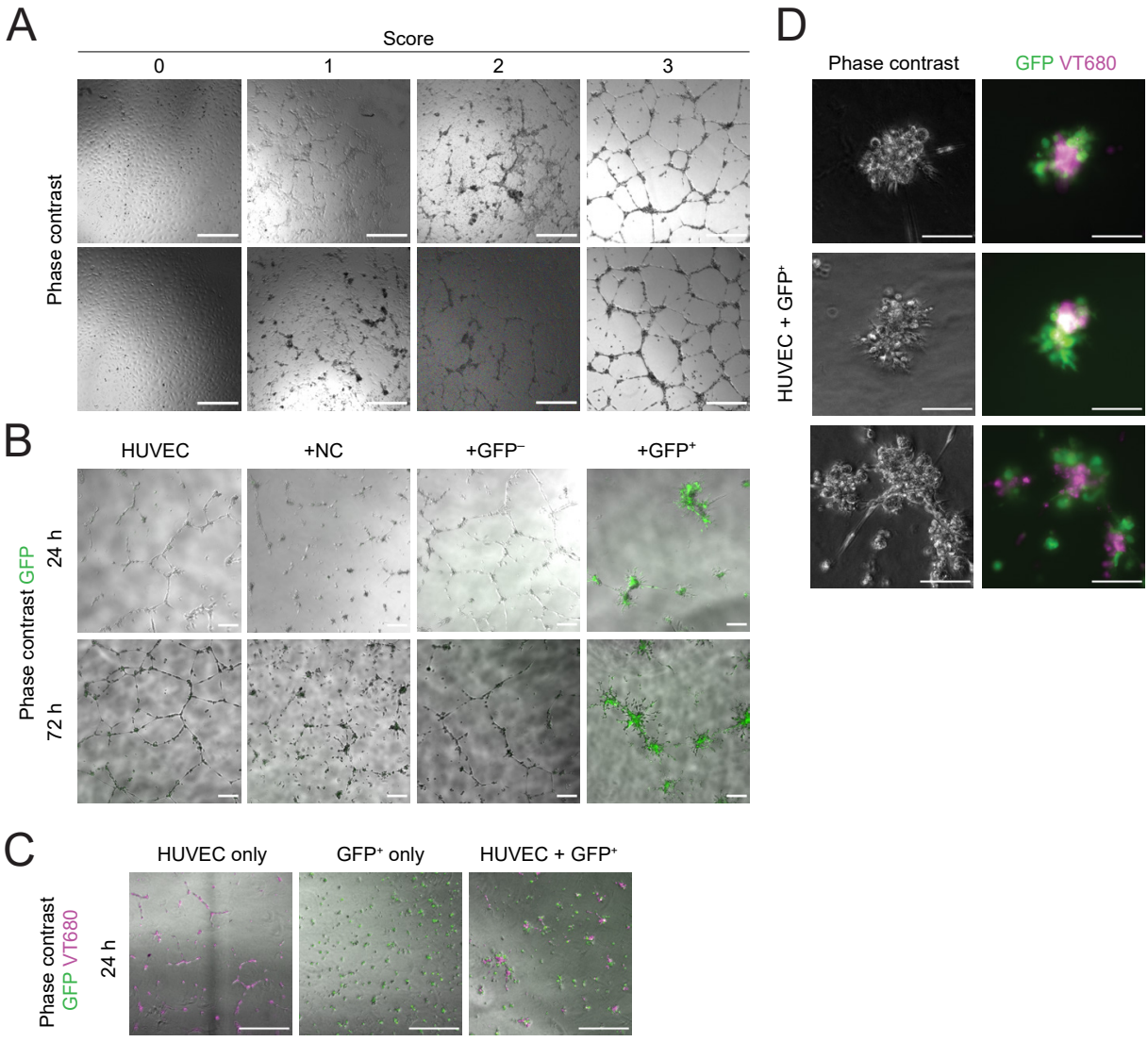

Figure S8. Cord formation assays. (A) Monoculture (HUVEC) cord formation assay scoring scheme. Example phase contrast images scored 0 (no cords apparent), 1 (few cords apparent, most cells not associated with cords), 2 (many cords apparent, most cells associated with cords), and 3 (virtually all cells associated with cords). Scale bars: 500 μm. **(B)** Coculture cord formation assay with HUVECs, HUVECs and neural crest cells (+NC), HUVECs and GFP^{-} cells from a N3ICD-GFP-transduced culture (5 days post-FACS; +GFP^{-}), and HUVECs and GFP^{+} cells from a N3ICD-GFP-transduced culture (5 days post-FACS; +GFP^{+}). Representative images (overlays of phase

contrast and GFP fluorescence) are shown from 24 h and 72 h after initiating assay, from a differentiation of the IMR90-4 hPSC line. Scale bars: 200 μm. **(C)** Coculture cord formation assay with HUVECs only, GFP^+ cells from a N3ICD-GFP-transduced culture only, and HUVECs and GFP^+ cells from a N3ICD-GFP-transduced culture (HUVEC + GFP^+). GFP^+ cells were used 5 days post-FACS. HUVECs were prelabeled with VivoTrack680 dye (VT680). Representative images (overlays of phase contrast, GFP fluorescence, and VT680 fluorescence) are shown from 24 h after initiating assay, from a differentiation of the H9 hPSC line. Scale bars: 500 μm. **(D)** High-magnification images of aggregates from the HUVEC + GFP^+ condition as described above. Scale bars: 100 μm.

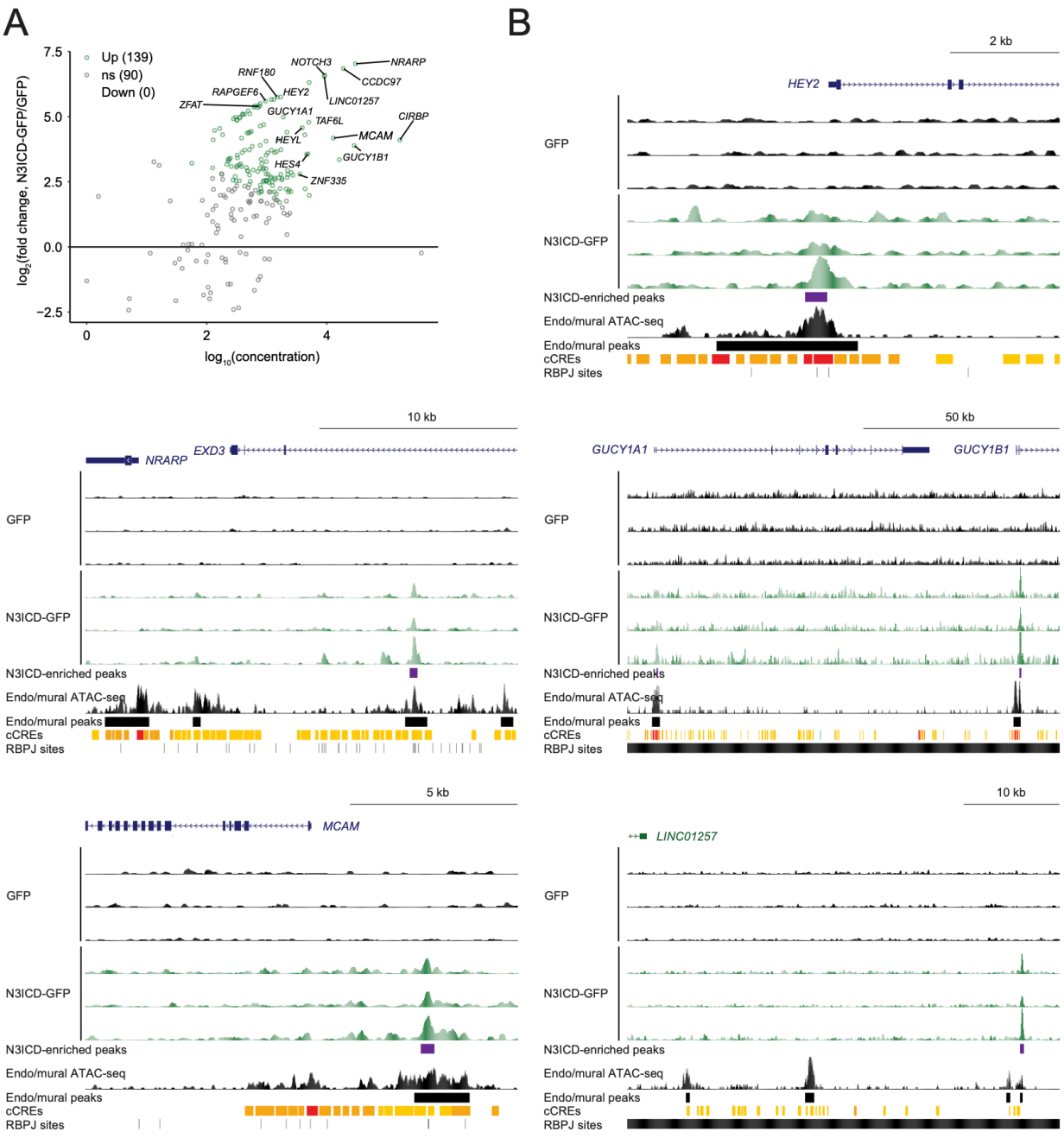

Figure S9. N3ICD-enriched peaks from Notch3 ChIP-seq. (A) Peak enrichment analysis of N3ICD-GFP-transduced cells compared to GFP-transduced cells. Data are displayed in a MA plot. N3ICD-enriched peaks (adjusted P-values < 0.05, DiffBind/DESeq2 Wald test with Benjamini-Hochberg correction) are highlighted in green, and the numbers of enriched (Up) and non-significant (ns) peaks are shown in the legend. Selected points are annotated with putative target

gene names. Complete results of peak enrichment analysis and peak annotation are provided in File S3. **(B)** Genome browser plots for genes of interest. From top, tracks are: Notch3 ChIP-seq signal from GFP-transduced cells (data from three differentiations), Notch ChIP-seq signal from N3ICD-GFP-transduced cells (data from three differentiations), N3ICD-enriched peaks as identified by DiffBind (purple bars), ATAC-seq signal from a human cortex endothelial/mural cell cluster (*66*), endothelial/mural ATAC-seq peaks as identified by MACS (*66*), ENCODE cCREs (red: promoter-like signature, orange: proximal enhancer-like signature, yellow: distal enhancer-like signature) (*67*), and putative RBPJ binding sites from the JASPAR database (*68*).

Descriptions of Files S1 to S3

- **File S1. RNA-seq transcript abundance data. (A,B)** RNA-seq data for hPSC-derived neural crest, GFP^-, and GFP^+ cells (this work, A) and hPSC-derived pericyte-like cells (literature data, B). Abundances are provided in transcripts per million (TPM). **(C)** Expression of protein-coding genes in mock bulk RNA-seq data from human brain pericytes (derived from scRNA-seq data from 5 studies), and bulk RNA-seq data from hPSC-derived brain pericyte-like cells (literature) and GFP^+ cells (this work) (see *Materials and Methods* and Table S1).
- **File S2. RNA-seq differential expression and pathway enrichment analysis. (A,B)** Differential expression analysis comparing GFP^+ cells to neural crest (A) and GFP^+ cells to GFP^- cells (B). For each gene, average expression (baseMean), $\log_2$(fold change), Wald statistic, P-value (Wald test), and adjusted P-value (Benjamini-Hochberg correction) derived from DESeq2 are shown. **(C)** List of genes in the 1110-gene module identified by hierarchical clustering as enriched in GFP^+ cells compared to both neural crest and GFP^- cells (Fig. S6C). **(D)** Pathways identified by Gene Set Enrichment Analysis as enriched in GFP^+ cells compared to neural crest. For each gene set, the database (KEGG or GO-BP), normalized enrichment score (NES), and false discovery rate (FDR) are shown.
- **File S3. Notch3 ChIP-seq peaks. (A)** Peaks called by MACS in each sample. **(B)** Peak enrichment results and peak annotations.

REFERENCES AND NOTES

1. A. Armulik, A. Abramsson, C. Betsholtz, Endothelial/pericyte interactions. *Circ. Res.* **97**, 512–523 (2005).

2. A. Armulik, G. Genové, C. Betsholtz, Pericytes: Developmental, physiological, and pathological perspectives, problems, and promises. *Dev. Cell* **21**, 193–215 (2011).

3. P. S. Hosford, I. N. Christie, A. Niranjan, Q. Aziz, N. Anderson, R. Ang, M. F. Lythgoe, J. A. Wells, A. Tinker, A. V. Gourine, A critical role for the ATP-sensitive potassium channel subunit KIR6.1 in the control of cerebral blood flow. *J. Cereb. Blood Flow Metab.* **39**, 2089–2095 (2019).

4. A. M. Nikolakopoulou, A. Montagne, K. Kisler, Z. Dai, Y. Wang, M. T. Huuskonen, A. P. Sagare, D. Lazic, M. D. Sweeney, P. Kong, M. Wang, N. C. Owens, E. J. Lawson, X. Xie, Z. Zhao, B. V. Zlokovic, Pericyte loss leads to circulatory failure and pleiotrophin depletion causing neuron loss. *Nat. Neurosci.* **22**, 1089–1098 (2019).

5. K. Kisler, A. M. Nikolakopoulou, M. D. Sweeney, D. Lazic, Z. Zhao, B. V. Zlokovic, Acute ablation of cortical pericytes leads to rapid neurovascular uncoupling. *Front. Cell. Neurosci.* **14**, 27 (2020).

6. K. Kisler, A. R. Nelson, S. V Rege, A. Ramanathan, Y. Wang, A. Ahuja, D. Lazic, P. S. Tsai, Z. Zhao, Y. Zhou, D. A. Boas, S. Sakadžić, B. V Zlokovic, Pericyte degeneration leads to neurovascular uncoupling and limits oxygen supply to brain. *Nat. Neurosci.* **20**, 406–416 (2017).

7. C. N. Hall, C. Reynell, B. Gesslein, N. B. Hamilton, A. Mishra, B. A. Sutherland, F. M. O'Farrell, A. M. Buchan, M. Lauritzen, D. Attwell, Capillary pericytes regulate cerebral blood flow in health and disease. *Nature* **508**, 55–60 (2014).

8. R. A. Hill, L. Tong, P. Yuan, S. Murikinati, S. Gupta, J. Grutzendler, Regional blood flow in the normal and ischemic brain is controlled by arteriolar smooth muscle cell contractility and not by capillary pericytes. *Neuron* **87**, 95–110 (2015).

9. C. M. Peppiatt, C. Howarth, P. Mobbs, D. Attwell, Bidirectional control of CNS capillary diameter by pericytes. *Nature* **443**, 700–704 (2006).

10. R. L. Rungta, E. Chaigneau, B.-F. F. Osmanski, S. Charpak, Vascular compartmentalization of functional hyperemia from the synapse to the Pia. *Neuron* **99**, 362–375.e4 (2018).

11. A. Armulik, G. Genové, M. Mäe, M. H. Nisancioglu, E. Wallgard, C. Niaudet, L. He, J. Norlin, P. Lindblom, K. Strittmatter, B. R. Johansson, C. Betsholtz, Pericytes regulate the blood–brain barrier. *Nature* **468**, 557–561 (2010).

12. R. D. Bell, E. A. Winkler, A. P. Sagare, I. Singh, B. LaRue, R. Deane, B. V. Zlokovic, Pericytes control key neurovascular functions and neuronal phenotype in the adult brain and during brain aging. *Neuron* **68**, 409–427 (2010).

13. R. Daneman, L. Zhou, A. A. Kebede, B. A. Barres, Pericytes are required for blood-brain barrier integrity during embryogenesis. *Nature* **468**, 562–566 (2010).

14. S. Grubb, C. Cai, B. O. Hald, L. Khennouf, R. P. Murmu, A. G. K. K. Jensen, J. Fordsmann, S. Zambach, M. Lauritzen, Precapillary sphincters maintain perfusion in the cerebral cortex. *Nat. Commun.* **11**, 395 (2020).

15. D. A. Hartmann, A. A. Berthiaume, R. I. Grant, S. A. Harrill, T. Koski, T. Tieu, K. P. McDowell, A. V. Faino, A. L. Kelly, A. Y. Shih, Brain capillary pericytes exert a substantial but slow influence on blood flow. *Nat. Neurosci.* **24**, 633–645 (2021).

16. M. Vanlandewijck, L. He, M. A. Mäe, J. Andrae, K. Ando, F. Del Gaudio, K. Nahar, T. Lebouvier, B. Laviña, L. Gouveia, Y. Sun, E. Raschperger, M. Räsänen, Y. Zarb, N. Mochizuki, A. Keller, U. Lendahl, C. Betsholtz, A molecular atlas of cell types and zonation in the brain vasculature. *Nature* **554**, 475–480 (2018).

17. R. I. Grant, D. A. Hartmann, R. G. Underly, A. A. Berthiaume, N. R. Bhat, A. Y. Shih, Organizational hierarchy and structural diversity of microvascular pericytes in adult mouse cortex. *J. Cereb. Blood Flow Metab.* **39**, 411–425 (2019).

18. D. A. Hartmann, V. Coelho-Santos, A. Y. Shih, Pericyte control of blood flow across microvascular zones in the central nervous system. *Annu. Rev. Physiol.* **84**, 331–354 (2022).

19. R. D. Bell, E. A. Winkler, I. Singh, A. P. Sagare, R. Deane, Z. Wu, D. M. Holtzman, C. Betsholtz, A. Armulik, J. Sallstrom, B. C. Berk, B. V. Zlokovic, Apolipoprotein e controls cerebrovascular integrity via cyclophilin A. *Nature* **485**, 512–516 (2012).

20. M. R. Halliday, S. V Rege, Q. Ma, Z. Zhao, C. A. Miller, E. A Winkler, B. V Zlokovic, Accelerated pericyte degeneration and blood-brain barrier breakdown in apolipoprotein E4 carriers with Alzheimer's disease. *J. Cereb. Blood Flow Metab.* **36**, 1–9 (2015).

21. R. Nortley, N. Korte, P. Izquierdo, C. Hirunpattarasilp, A. Mishra, Z. Jaunmuktane, V. Kyrargyri, T. Pfeiffer, L. Khennouf, C. Madry, H. Gong, A. Richard-Loendt, W. Huang, T. Saito, T. C. Saido, S. Brandner, H. Sethi, D. Attwell, Amyloid β oligomers constrict human capillaries in Alzheimer's disease via signaling to pericytes. *Science* **365**, eaav9518 (2019).

22. A. Joutel, F. Andreux, S. Gaulis, V. Domenga, M. Cecillon, N. Battail, N. Piga, F. Chapon, C. Godfrain, E. Tournier-Lasserve, The ectodomain of the Notch3 receptor accumulates within the cerebrovasculature of CADASIL patients. *J. Clin. Invest.* **105**, 597–605 (2000).

23. M. Ghosh, M. Balbi, F. Hellal, M. Dichgans, U. Lindauer, N. Plesnila, Pericytes are involved in the pathogenesis of cerebral autosomal dominant arteriopathy with subcortical infarcts and leukoencephalopathy. *Ann. Neurol.* **78**, 887–900 (2015).

24. H. C. Etchevers, C. Vincent, N. M. Le Douarin, G. F. Couly, The cephalic neural crest provides pericytes and smooth muscle cells to all blood vessels of the face and forebrain. *Development* **128**, 1059–1068 (2001).

25. J. Korn, B. Christ, R. Kurz, H. Kurz, R. Kurz, H. Kurz, R. Kurz, H. Kurz, Neuroectodermal origin of brain pericytes and vascular smooth muscle cells. *J. Comp. Neurol.* **442**, 78–88 (2002).

26. E. Yamanishi, M. Takahashi, Y. Saga, N. Osumi, Penetration and differentiation of cephalic neural crest-derived cells in the developing mouse telencephalon. *Dev. Growth Differ.* **54**, 785–800 (2012).

27. C. S. Le Lièvre, N. M. Le Douarin, Mesenchymal derivatives of the neural crest: Analysis of chimaeric quail and chick embryos. *J. Embryol. Exp. Morphol.* **34**, 125–154 (1975).

28. H. C. Etchevers, G. Couly, C. Vincent, N. M. Le Douarin, Anterior cephalic neural crest is required for forebrain viability. *Development* **126**, 3533–3543 (1999).

29. X. Jiang, S. Iseki, R. E. Maxson, H. M. Sucov, G. M. Morriss-Kay, Tissue origins and interactions in the mammalian skull vault. *Dev. Biol.* **241**, 106–116 (2002).

30. P. Lindahl, B. R. Johansson, P. Levéen, C. Betsholtz, Pericyte loss and microaneurysm formation in PDGF-B-deficient mice. *Science* **277**, 242–245 (1997).

31. M. Hellström, M. Kalén, P. Lindahl, A. Abramsson, C. Betsholtz, Role of PDGF-B and PDGFR-beta in recruitment of vascular smooth muscle cells and pericytes during embryonic blood vessel formation in the mouse. *Development* **126**, 3047–3055 (1999).

32. K. Ando, W. Wang, D. Peng, A. Chiba, A. K. Lagendijk, L. Barske, J. G. Crump, D. Y. R. R. Stainier, U. Lendahl, K. Koltowska, B. M. Hogan, S. Fukuhara, N. Mochizuki, C. Betsholtz, Peri-arterial specification of vascular mural cells from naïve mesenchyme requires Notch signaling. *Development* **146**, dev165589 (2019).

33. Y. Wang, L. Pan, C. B. Moens, B. Appel, Notch3 establishes brain vascular integrity by regulating pericyte number. *Development* **141**, 307–317 (2014).

34. H. Wurdak, Inactivation of TGFβ signaling in neural crest stem cells leads to multiple defects reminiscent of DiGeorge syndrome. *Genes Dev.* **19**, 530–535 (2005).

35. T. L. Henshall, A. Keller, L. He, B. R. Johansson, E. Wallgard, E. Raschperger, M. A. Mäe, S. Jin, C. Betsholtz, U. Lendahl, Notch3 is necessary for blood vessel integrity in the central nervous system. *Arterioscler. Thromb. Vasc. Biol.* **35**, 409–420 (2015).

36. T. Nadeem, W. Bogue, B. Bigit, H. Cuervo, Deficiency of Notch signaling in pericytes results in arteriovenous malformations. *JCI Insight* **5**, e125940 (2020).

37. N. M. Shah, A K. Groves, D. J. Anderson, Alternative neural crest cell fates are instructively promoted by TGFbeta superfamily members. *Cell* **85**, 331–343 (1996).

38. L. Menendez, T. A. Yatskievych, P. B. Antin, S. Dalton, L. Menendez, T. A. Yatskievych, P. B. Antin, S. Dalton, Wnt signaling and a Smad pathway blockade direct the differentiation of human pluripotent stem cells to multipotent neural crest cells. *Proc. Natl. Acad. Sci. U.S.A.* **109**, 9220 (2012).

39. G. Lee, H. Kim, Y. Elkabetz, G. Al Shamy, G. Panagiotakos, T. Barberi, V. Tabar, L. Studer, Isolation and directed differentiation of neural crest stem cells derived from human embryonic stem cells. *Nat. Biotechnol.* **25**, 1468–1475 (2007).

40. H. W. Song, K. L. Foreman, B. D. Gastfriend, J. S. Kuo, S. P. Palecek, E. V. Shusta, Transcriptomic comparison of human and mouse brain microvessels. *Sci. Rep.* **10**, 12358 (2020).

41. B. D. Gastfriend, K. L. Foreman, M. E. Katt, S. P. Palecek, E. V. Shusta, Integrative analysis of the human brain mural cell transcriptome. *J. Cereb. Blood Flow Metab.* **41**, 3052–3068 (2021).

42. B. D. Gastfriend, S. P. Palecek, E. V Shusta, Modeling the blood–brain barrier: Beyond the endothelial cells. *Curr. Opin. Biomed. Eng.* **5**, 6–12 (2018).

43. M. J. Stebbins, B. D. Gastfriend, S. G. Canfield, M.-S. S. Lee, D. Richards, M. G. Faubion, W.-J. J. Li, R. Daneman, S. P. Palecek, E. V. Shusta, Human pluripotent stem cell–derived brain pericyte–like cells induce blood-brain barrier properties. *Sci. Adv.* **5**, eaau7375 (2019).

44. B. D. Gastfriend, M. J. Stebbins, F. Du, E. V. Shusta, S. P. Palecek, Differentiation of brain pericyte-like cells from human pluripotent stem cell−derived neural crest. *Curr. Protoc.* **1**, e21 (2021).

45. C. Griffin, R. Bajpai, Neural crest-derived human cranial pericytes model primary forebrain pericytes and predict disease-specific cranial vasculature defects. *SSRN Electron. J.* (2017).

46. J. Sun, Y. Huang, J. Gong, J. Wang, Y. Fan, J. Cai, Y. Wang, Y. Qiu, Y. Wei, C. Xiong, J. Chen, B. Wang, Y. Ma, L. Huang, X. Chen, S. Zheng, W. Huang, Q. Ke, T. Wang, X. Li, W. Zhang, A. P. Xiang, W. Li, Transplantation of hPSC-derived pericyte-like cells promotes functional recovery in ischemic stroke mice. *Nat. Commun.* **11**, 5196 (2020).

47. K. Ando, L. Tong, D. Peng, E. Vázquez-Liébanas, H. Chiyoda, L. He, J. Liu, K. Kawakami, N. Mochizuki, S. Fukuhara, J. Grutzendler, C. Betsholtz, KCNJ8/ABCC9-containing K-ATP channel modulates brain vascular smooth muscle development and neurovascular coupling. *Dev. Cell* **57**, 1383–1399.e7 (2022).

48. G. La Manno, K. Siletti, A. Furlan, D. Gyllborg, E. Vinsland, A. Mossi Albiach, C. Mattsson Langseth, I. Khven, A. R. Lederer, L. M. Dratva, A. Johnsson, M. Nilsson, P. Lönnerberg, S. Linnarsson, Molecular architecture of the developing mouse brain. *Nature* **596**, 92–96 (2021).

49. R. Lehal, J. Zaric, M. Vigolo, C. Urech, V. Frismantas, N. Zangger, L. Cao, A. Berger, I. Chicote, S. Loubéry, S. H. Choi, U. Koch, S. C. Blacklow, H. G. Palmer, B. Bornhauser, M. González-Gaitán, Y. Arsenijevic, V. Zoete, J. C. Aster, J. P. Bourquin, F. Radtke, Pharmacological disruption of the Notch transcription factor complex. *Proc. Natl. Acad. Sci. U.S.A.* **117**, 16292–16301 (2020).

50. R. Soldatov, M. Kaucka, M. E. Kastriti, J. Petersen, T. Chontorotzea, L. Englmaier, N. Akkuratova, Y. Yang, M. Häring, V. Dyachuk, C. Bock, M. Farlik, M. L. Piacentino, F. Boismoreau, M. M. Hilscher, C. Yokota, X. Qian, M. Nilsson, M. E. Bronner, L. Croci, W.-Y. Y. Hsiao, D. A. Guertin, J.-F. F. Brunet, G. G. Consalez, P. Ernfors, K. Fried, P. V. Kharchenko, I. Adameyko, Spatiotemporal structure of cell fate decisions in murine neural crest. *Science* **364**, eaas9536 (2019).

51. J. A. Siegenthaler, Y. Choe, K. P. Patterson, I. Hsieh, D. Li, S.-C. S.-C. C. Jaminet, R. Daneman, T. Kume, E. J. Huang, S. J. Pleasure, Foxc1 is required by pericytes during fetal brain angiogenesis. *Biol. Open* **2**, 647–659 (2013).

52. A. Reyahi, A. M. Nik, M. Ghiami, A. Gritli-Linde, F. Pontén, B. R. Johansson, P. Carlsson, Foxf2 is required for brain pericyte differentiation and development and maintenance of the blood-brain barrier. *Dev. Cell* **34**, 19–32 (2015).

53. D. Bhattacharya, M. Rothstein, A. P. Azambuja, M. Simoes-Costa, Control of neural crest multipotency by Wnt signaling and the Lin28/let-7 axis. *eLife* **7**, e40556 (2018).

54. A. C. Yang, R. T. Vest, F. Kern, D. P. Lee, M. Agam, C. A. Maat, P. M. Losada, M. B. Chen, N. Schaum, N. Khoury, A. Toland, K. Calcuttawala, H. Shin, R. Pálovics, A. Shin, E. Y. Wang, J. Luo, D. Gate, W. J. Schulz-Schaeffer, P. Chu, J. A. Siegenthaler, M. W. McNerney, A. Keller, T. Wyss-Coray, A human brain vascular atlas reveals diverse mediators of Alzheimer's risk. *Nature* **603**, 885–892 (2022).

55. L. Muhl, G. Genové, S. Leptidis, J. Liu, L. He, G. Mocci, Y. Sun, S. Gustafsson, B. Buyandelger, I. V Chivukula, Å. Segerstolpe, E. Raschperger, E. M. Hansson, J. L. M. Björkegren, X. Peng, M. Vanlandewijck, U. Lendahl, C. Betsholtz, Single-cell analysis uncovers fibroblast heterogeneity and criteria for fibroblast and mural cell identification and discrimination. *Nat. Commun.* **11**, 3953 (2020).

56. J. DeSisto, R. O'Rourke, H. E. Jones, B. Pawlikowski, A. D. Malek, S. Bonney, F. Guimiot, K. L. Jones, J. A. Siegenthaler, Single-cell transcriptomic analyses of the developing meninges reveal meningeal fibroblast diversity and function. *Dev. Cell* **54**, 43–59.e4 (2020).

57. F. J. Garcia, N. Sun, H. Lee, B. Godlewski, H. Mathys, K. Galani, B. Zhou, X. Jiang, A. P. Ng, J. Mantero, L.-H. Tsai, D. A. Bennett, M. Sahin, M. Kellis, M. Heiman, Single-cell dissection of the human brain vasculature. *Nature* **603**, 893–899 (2022).

58. Y. Kubota, H. K. Kleinman, G. R. Martin, T. J. Lawley, Role of laminin and basement membrane in the morphological differentiation of human endothelial cells into capillary-like structures. *J. Cell Biol.* **107**, 1589–1598 (1988).

59. A. Kumar, S. S. D'Souza, O. V. Moskvin, H. Toh, B. Wang, J. Zhang, S. Swanson, L. W. Guo, J. A. Thomson, I. I. Slukvin, Specification and diversification of pericytes and smooth muscle cells from mesenchymoangioblasts. *Cell Rep.* **19**, 1902–1916 (2017).

60. B. Lilly, S. Kennard, Differential gene expression in a coculture model of angiogenesis reveals modulation of select pathways and a role for Notch signaling. *Physiol. Genomics* **36**, 69–78 (2009).

61. A. L. Gonzales, N. R. Klug, A. Moshkforoush, J. C. Lee, F. K. Lee, B. Shui, N. M. Tsoukias, M. I. Kotlikoff, D. Hill-Eubanks, M. T. Nelson, Contractile pericytes determine the direction of blood flow at capillary junctions. *Proc. Natl. Acad. Sci. U.S.A.* **117**, 27022–27033 (2020).

62. S. A. Zambach, C. Cai, H. C. C. Helms, B. O. Hald, Y. Dong, J. C. Fordsmann, R. M. Nielsen, J. Hu, M. Lønstrup, B. Brodin, M. J. Lauritzen, Precapillary sphincters and pericytes at first-order capillaries as key regulators for brain capillary perfusion. *Proc. Natl. Acad. Sci. U.S.A.* **118**, e2023749118 (2021).

63. S. J. Bray, M. Gomez-Lamarca, Notch after cleavage. *Curr. Opin. Cell Biol.* **51**, 103–109 (2018).

64. R. Stark, G. Brown, DiffBind: Differential binding analysis of ChIP-Seq peak data; http://bioconductor.org/packages/release/bioc/vignettes/DiffBind/inst/doc/DiffBind.pdf.

65. D. Castel, P. Mourikis, S. J. J. J. Bartels, A. B. Brinkman, S. Tajbakhsh, H. G. Stunnenberg, Dynamic binding of RBPJ is determined by notch signaling status. *Genes Dev.* **27**, 1059–1071 (2013).

66. R. S. Ziffra, C. N. Kim, J. M. Ross, A. Wilfert, T. N. Turner, M. Haeussler, A. M. Casella, P. F. Przytycki, K. C. Keough, D. Shin, D. Bogdanoff, A. Kreimer, K. S. Pollard, S. A. Ament,

E. E. Eichler, N. Ahituv, T. J. Nowakowski, Single-cell epigenomics reveals mechanisms of human cortical development. *Nature* **598**, 205–213 (2021).

67. Y. Luo, B. C. Hitz, I. Gabdank, J. A. Hilton, M. S. Kagda, B. Lam, Z. Myers, P. Sud, J. Jou, K. Lin, U. K. Baymuradov, K. Graham, C. Litton, S. R. Miyasato, J. S. Strattan, O. Jolanki, J. W. Lee, F. Y. Tanaka, P. Adenekan, E. O'Neill, J. M. Cherry, New developments on the Encyclopedia of DNA Elements (ENCODE) data portal. *Nucleic Acids Res.* **48**, D882–D889 (2020).

68. J. A. Castro-Mondragon, R. Riudavets-Puig, I. Rauluseviciute, R. B. Lemma, L. Turchi, R. Blanc-Mathieu, J. Lucas, P. Boddie, A. Khan, N. M. Pérez, O. Fornes, T. Y. Leung, A. Aguirre, F. Hammal, D. Schmelter, D. Baranasic, B. Ballester, A. Sandelin, B. Lenhard, K. Vandepoele, W. W. Wasserman, F. Parcy, A. Mathelier, JASPAR 2022: The 9th release of the open-access database of transcription factor binding profiles. *Nucleic Acids Res.* **50**, D165–D173 (2022).

69. S. Chen, R. J. Lechleider, Transforming growth factor-beta-induced differentiation of smooth muscle from a neural crest stem cell line. *Circ. Res.* **94**, 1195–1202 (2004).

70. K. K. Hirschi, S. A. Rohovsky, P. A. D'Amore, PDGF, TGF-beta, and heterotypic cell-cell interactions mediate endothelial cell-induced recruitment of 10T1/2 cells and their differentiation to a smooth muscle fate. *J. Cell Biol.* **141**, 805–814 (1998).

71. L. He, M. Vanlandewijck, E. Raschperger, M. Andaloussi Mäe, B. Jung, T. Lebouvier, K. Ando, J. Hofmann, A. Keller, C. Betsholtz, Analysis of the brain mural cell transcriptome. *Sci. Rep.* **6**, 35108 (2016).

72. C. Cheung, A. S. Bernardo, M. W. B. Trotter, R. A. Pedersen, S. Sinha, Generation of human vascular smooth muscle subtypes provides insight into embryological origin–dependent disease susceptibility. *Nat. Biotechnol.* **30**, 165–173 (2012).

73. C. Cheung, Y. T. Goh, J. Zhang, C. Wu, E. Guccione, Modeling cerebrovascular pathophysiology in amyloid-β metabolism using neural-crest-derived smooth muscle cells. *Cell Rep.* **9**, 391–401 (2014).

74. C. Patsch, L. Challet-Meylan, E. C. Thoma, E. Urich, T. Heckel, J. F. O'Sullivan, S. J. Grainger, F. G. Kapp, L. Sun, K. Christensen, Y. Xia, M. H. C. Florido, W. He, W. Pan, M. Prummer, C. R. Warren, R. Jakob-Roetne, U. Certa, R. Jagasia, P. O. Freskgard, I. Adatto, D. Kling, P. Huang, L. I. Zon, E. L. Chaikof, R. E. Gerszten, M. Graf, R. Iacone, C. A. Cowan, Generation of vascular endothelial and smooth muscle cells from human pluripotent stem cells. *Nat. Cell Biol.* **17**, 994–1003 (2015).

75. T. Faal, D. T. T. T. Phan, H. Davtyan, V. M. Scarfone, E. Varady, C. C. W. W. Hughes, M. A. Inlay, M. Blurton-Jones, C. C. W. W. Hughes, M. A. Inlay, Induction of mesoderm and neural crest-derived pericytes from human pluripotent stem cells to study blood-brain barrier interactions. *Stem Cell Reports* **12**, 451–460 (2019).

76. L. A. Brown, P. Sava, C. Garcia, A. L. Gonzalez, N. Haven, L. A. Brown, P. Sava, C. Garcia, A. L. Gonzalez, N. Haven, Proteomic analysis of the pericyte derived extracellular matrix. *Cell. Mol. Bioeng.* **8**, 349–363 (2015).

77. A. Montagne, A. M. Nikolakopoulou, Z. Zhao, A. P. Sagare, G. Si, D. Lazic, S. R. Barnes, M. Daianu, A. Ramanathan, A. Go, E. J. Lawson, Y. Wang, W. J. Mack, P. M. Thompson, J. A. Schneider, J. Varkey, R. Langen, E. Mullins, R. E. Jacobs, B. V. Zlokovic, Pericyte degeneration causes white matter dysfunction in the mouse central nervous system. *Nat. Med.* **24**, 326–337 (2018).

78. J. W. Blanchard, M. Bula, J. Davila-Velderrain, L. A. Akay, L. Zhu, A. Frank, M. B. Victor, J. M. Bonner, H. Mathys, Y. T. Lin, T. Ko, D. A. Bennett, H. P. Cam, M. Kellis, L. H. Tsai, Reconstruction of the human blood–brain barrier in vitro reveals a pathogenic mechanism of APOE4 in pericytes. *Nat. Med.* **26**, 952–963 (2020).

79. B. D. Gastfriend, H. Nishihara, S. G. Canfield, K. L. Foreman, B. Engelhardt, S. P. Palecek, E. V Shusta, Wnt signaling mediates acquisition of blood–brain barrier properties in naïve endothelium derived from human pluripotent stem cells. *eLife* **10**, 70992 (2021).

80. H. Nishihara, S. Perriot, B. D. Gastfriend, M. Steinfort, C. Cibien, S. Soldati, K. Matsuo, S. Guimbal, A. Mathias, S. P. Palecek, E. V Shusta, R. Du Pasquier, B. Engelhardt, Intrinsic blood-brain barrier dysfunction contributes to multiple sclerosis pathogenesis. *Brain* **145**, 4334–4348 (2022).

81. J. A. Thomson, Embryonic stem cell lines derived from human blastocysts. *Science* **282**, 1145–1147 (1998).

82. J. Yu, M. A. Vodyanik, K. Smuga-Otto, J. Antosiewicz-Bourget, J. L. Frane, S. Tian, J. Nie, G. A. Jonsdottir, V. Ruotti, R. Stewart, I. I. Slukvin, J. A. Thomson, Induced pluripotent stem cell lines derived from human somatic cells. *Science* **1917**, 154–155 (2008).

83. J. Yu, K. Hu, K. Smuga-Otto, S. Tian, R. Stewart, I. I. Slukvin, J. A. Thomson, Human induced pluripotent stem cells free of vector and transgene sequences. *Science* **324**, 797–801 (2009).

84. F. R. Kreitzer, N. Salomonis, A. Sheehan, M. Huang, J. S. Park, M. J. Spindler, P. Lizarraga, W. A. Weiss, P. So, B. R. Conklin, A robust method to derive functional neural crest cells from human pluripotent stem cells. *Am. J. Stem Cells* **2**, 119–131 (2013).

85. G. Chen, D. R. Gulbranson, Z. Hou, J. M. Bolin, V. Ruotti, M. D. Probasco, K. Smuga-Otto, S. E. Howden, N. R. Diol, N. E. Propson, R. Wagner, G. O. Lee, J. Antosiewicz-Bourget, J. M. C. Teng, J. A. Thomson, Chemically defined conditions for human iPSC derivation and culture. *Nat. Methods* **8**, 424–429 (2011).

86. A. Dobin, C. A. Davis, F. Schlesinger, J. Drenkow, C. Zaleski, S. Jha, P. Batut, M. Chaisson, T. R. Gingeras, STAR: Ultrafast universal RNA-seq aligner. *Bioinformatics* **29**, 15–21 (2013).

87. Y. Liao, G. K. Smyth, W. Shi, FeatureCounts: An efficient general purpose program for assigning sequence reads to genomic features. *Bioinformatics* **30**, 923–930 (2014).

88. R. D. Hodge, T. E. Bakken, J. A. Miller, K. A. Smith, E. R. Barkan, L. T. Graybuck, J. L. Close, B. Long, N. Johansen, O. Penn, Z. Yao, J. Eggermont, T. Höllt, B. P. Levi, S. I. Shehata, B. Aevermann, A. Beller, D. Bertagnolli, K. Brouner, T. Casper, C. Cobbs, R. Dalley, N. Dee, S. L. Ding, R. G. Ellenbogen, O. Fong, E. Garren, J. Goldy, R. P. Gwinn, D. Hirschstein, C. D. Keene, M. Keshk, A. L. Ko, K. Lathia, A. Mahfouz, Z. Maltzer, M. McGraw, T. N. Nguyen, J. Nyhus, J. G. Ojemann, A. Oldre, S. Parry, S. Reynolds, C. Rimorin, N. V. Shapovalova, S. Somasundaram, A. Szafer, E. R. Thomsen, M. Tieu, G. Quon, R. H. Scheuermann, R. Yuste, S. M. Sunkin, B. Lelieveldt, D. Feng, L. Ng, A. Bernard, M. Hawrylycz, J. W. Phillips, B. Tasic, H. Zeng, A. R. Jones, C. Koch, E. S. Lein, Conserved cell types with divergent features in human versus mouse cortex. *Nature* **573**, 61–68 (2019).

89. D. Polioudakis, L. de la Torre-Ubieta, J. Langerman, A. G. Elkins, X. Shi, J. L. Stein, C. K. Vuong, S. Nichterwitz, M. Gevorgian, C. K. Opland, D. Lu, W. Connell, E. K. Ruzzo, J. K. Lowe, T. Hadzic, F. I. Hinz, S. Sabri, W. E. Lowry, M. B. Gerstein, K. Plath, D. H. Geschwind, A single-cell transcriptomic atlas of human neocortical development during mid-gestation. *Neuron* **103**, 785–801.e8 (2019).

90. G. La Manno, D. Gyllborg, S. Codeluppi, K. Nishimura, C. Salto, A. Zeisel, L. E. Borm, S. R. W. Stott, E. M. Toledo, J. C. Villaescusa, P. Lönnerberg, J. Ryge, R. A. Barker, E. Arenas, S. Linnarsson, Molecular diversity of midbrain development in mouse, human, and stem cells. *Cell* **167**, 566–580.e19 (2016).

91. X. Han, Z. Zhou, L. Fei, H. Sun, R. Wang, Y. Chen, H. Chen, J. Wang, H. Tang, W. Ge, Y. Zhou, F. Ye, M. Jiang, J. Wu, Y. Xiao, X. Jia, T. Zhang, X. Ma, Q. Zhang, X. Bai, S. Lai, C. Yu, L. Zhu, R. Lin, Y. Gao, M. Wang, Y. Wu, J. Zhang, R. Zhan, S. Zhu, H. Hu, C. Wang, M. Chen, H. Huang, T. Liang, J. Chen, W. Wang, D. Zhang, G. Guo, Construction of a human cell landscape at single-cell level. *Nature* **581**, 303–309 (2020).

92. S. Zhong, W. Ding, L. Sun, Y. Lu, H. Dong, X. Fan, Z. Liu, R. Chen, S. Zhang, Q. Ma, F. Tang, Q. Wu, X. Wang, Decoding the development of the human hippocampus. *Nature* **577**, 531–536 (2020).

93. M. I. Love, W. Huber, S. Anders, Moderated estimation of fold change and dispersion for RNA-seq data with DESeq2. *Genome Biol.* **15**, 550 (2014).

94. A. Subramanian, P. Tamayo, V. K. Mootha, S. Mukherjee, B. L. Ebert, M. A. Gillette, A. Paulovich, S. L. Pomeroy, T. R. Golub, E. S. Lander, J. P. Mesirov, Gene set enrichment analysis: A knowledge-based approach for interpreting genome-wide expression profiles. *Proc. Natl. Acad. Sci. U.S.A.* **102**, 15545–15550 (2005).

95. M. Kanehisa, S. Goto, KEGG: Kyoto encyclopedia of genes and genomes. *Nucleic Acids Res.* **28**, 27–30 (2000).

96. The Gene Ontology Consortium; M. Ashburner, C. A. Ball, J. A. Blake, D. Botstein, H. Butler, J. M. Cherry, A. P. Davis, K. Dolinski, S. S. Dwight, J. T. Eppig, M. A. Harris, D. P. Hill, L. Issel-Tarver, A. Kasarskis, S. Lewis, J. C. Matese, J. E. Richardson, M. Ringwald, G. M. Rubin, G. Sherlock, Gene ontology: Tool for the unification of biology. *Nat. Genet.* **25**, 25–29 (2000).

97. J. T. Robinson, H. Thorvaldsdóttir, W. Winckler, M. Guttman, E. S. Lander, G. Getz, J. P. Mesirov, Integrative genomics viewer. *Nat. Biotechnol.* **29**, 24–26 (2011).

98. F. A. Wolf, P. Angerer, F. J. Theis, SCANPY: Large-scale single-cell gene expression data analysis. *Genome Biol.* **19**, 15 (2018).

99. M. E. Floy, S. E. Givens, O. B. Matthys, T. D. Mateyka, C. M. Kerr, A. B. Steinberg, A. C. Silva, J. Zhang, Y. Mei, B. M. Ogle, T. C. McDevitt, T. J. Kamp, S. P. Palecek, Developmental lineage of human pluripotent stem cell-derived cardiac fibroblasts affects their functional phenotype. *FASEB J.* **35**, e21799 (2021).

100. J. Schindelin, I. Arganda-Carreras, E. Frise, V. Kaynig, M. Longair, T. Pietzsch, S. Preibisch, C. Rueden, S. Saalfeld, B. Schmid, J. Tinevez, D. J. White, V. Hartenstein, K.

Eliceiri, P. Tomancak, A. Cardona, Fiji: An open-source platform for biological-image analysis. *Nat. Methods* **9**, 676–682 (2012).

101. B. Langmead, S. L. Salzberg, Fast gapped-read alignment with Bowtie 2. *Nat. Methods* **9**, 357–359 (2012).

102. A. Tarasov, A. J. Vilella, E. Cuppen, I. J. Nijman, P. Prins, Sambamba: Fast processing of NGS alignment formats. *Bioinformatics* **31**, 2032–2034 (2015).

103. A. R. Quinlan, I. M. Hall, BEDTools: A flexible suite of utilities for comparing genomic features. *Bioinformatics* **26**, 841–842 (2010).

104. H. M. Amemiya, A. Kundaje, A. P. Boyle, The ENCODE Blacklist: Identification of problematic regions of the genome. *Sci. Rep.* **9**, 9354 (2019).

105. Y. Zhang, T. Liu, C. A. Meyer, J. Eeckhoute, D. S. Johnson, B. E. Bernstein, C. Nussbaum, R. M. Myers, M. Brown, W. Li, X. S. Shirley, Model-based analysis of ChIP-Seq (MACS). *Genome Biol.* **9**, R137 (2008).

106. G. Yu, L. G. Wang, Q. Y. He, ChIPseeker: An R/Bioconductor package for ChIP peak annotation, comparison and visualization. *Bioinformatics* **31**, 2382–2383 (2015).

107. F. Ramírez, D. P. Ryan, B. Grüning, V. Bhardwaj, F. Kilpert, A. S. Richter, S. Heyne, F. Dündar, T. Manke, deepTools2: A next generation web server for deep-sequencing data analysis. *Nucleic Acids Res.* **44**, W160–W165 (2016).

108. P. Machanick, T. L. Bailey, MEME-ChIP: Motif analysis of large DNA datasets. *Bioinformatics* **27**, 1696–1697 (2011).

109. W. J. Kent, C. W. Sugnet, T. S. Furey, K. M. Roskin, T. H. Pringle, A. M. Zahler, D. Haussler, The human genome browser at UCSC. *Genome Res.* **12**, 996–1006 (2002).

110. J. L. Everson, D. M. Fink, J. W. Yoon, E. J. Leslie, H. W. Kietzman, L. J. Ansen-Wilson, H. M. Chung, D. O. Walterhouse, M. L. Marazita, R. J. Lipinski, Sonic hedgehog regulation

of *Foxf2* promotes cranial neural crest mesenchyme proliferation and is disrupted in cleft lip morphogenesis. *Development* **144**, 2082–2091 (2017).